ADVANCED DIAGNOSTICS FOR MEGAHERTZ IMAGING OF MIXING, FUEL SPRAY, AND COMBUSTION PROCESSES FOR ROTATING DETONATION COMBUSTORS

C.A. Fugger, N. Jiang, P. Hsu, M. Slipchenko, S. Roy
Spectral Energies, LLC
Beavercreek, Ohio

H.D. Perkins
NASA Glenn Research Center
Cleveland, Ohio

T.R. Meyer, C.D. Slabaugh, G. Paniagua, V. Athmanathan, A. M. Webb, Z. Ayers, M.W. Hoeper, R.B. Wang, A. Lemcherfi, R.M. Gejji, E.W. Plaehn, J. Braun
Purdue University
West Lafayette, Indiana

ABSTRACT

Recent advancements in megahertz rate, high-power, burst-mode laser technology are leveraged to perform and explore imaging measurements that spatially and temporally resolve the mixing, combustion, and detonation flow field in two laboratory-scale rotating detonation combustors (RDCs). In a non-premixed annular RDC, multiple imaging diagnostics are explored to investigate gaseous and liquid injector behavior, the detonation wave structure, and the propellant refill. In one instance, OH planar laser-induced fluorescence (OH-PLIF) imaging is performed up to a 2 MHz repetition rate to track the combustion products and reaction zone locations. In the same annular RDC, a single liquid fuel jet is injected, and laser-based 355-nm imaging of the fuel spray is performed up to a 1 MHz repetition rate. For this configuration, the annular RDC is used as a detonation driver to impose periodic detonation waves to interact with the fuel spray. Moreover in this annular RDC, a range of tracer-based laser imaging measurements are explored to time-resolve the unsteady oxidizer air recovery and refill process. In a non-premixed linear RDC, planar imaging measurements of the fuel mixing are performed up to a 200 kHz repetition rate using PLIF of a tracer in the fuel supply. The fuel mixing imaging helps explain the origin of the observed pre and post wave burning, detonation structure, and enables quantifying injector recovery timescales. This paper will provide a high-level broad survey of diagnostics applied in these RDCs, lessons learned, and interesting observations.

INTRODUCTION

The rotating detonation engine (RDE) is of significant interest for its potential to improve the thermodynamic efficiency of combustion systems [1]. For many rotating detonation combustors (RDCs) currently being investigated, non-premixed reactants are injected at an annulus inlet, and after fuel-oxidizer mixing, a detonation wave propagates azimuthally around the annulus consuming the reactants with large and rapid pressure and temperature increases [2, 3]. The flowfield is highly unsteady and periodic, with detonation waves typically propagating at speeds of 1–2 km/s. Periodic reactant refill-combustion cycle times of ~30–500 μs can occur for single or multiple detonation wave cases, with secondary shock wave phenomena potentially affecting the reactant dynamics and local temperatures and pressures within the system [4, 5]. Although RDEs represent a promising new approach, the a priori design and optimization of the injection processes are difficult to perform as many of the gas dynamic, combustion, and coupled effects

are not yet well understood, particularly for the case of liquid-based systems that also include multiphase phenomena.

For fuel and oxidizer injection processes, the periodic high-pressure detonation impulses lead to highly unsteady reactant inlet dynamics, greatly affecting the local detonation wave characteristics. The majority of prior RDC studies have been performed using gas-gas RDCs. Based on numerical simulations and *very limited* experimental measurements, the effects of the detonation wave include reactant injection cessation into the combustor channel for as much as 25% of the detonation period, unequal injection recovery times of the fuel and oxidizer, non-ideal reactant mixing, and reactant-product mixing [6–10]. These effects lead to deflagration upstream of the detonation wave and/or incomplete combustion of the fuel [8, 11]. Resolving these processes experimentally and understanding the highly coupled underlying physics are inherently difficult as they occur on timescales that are much smaller than the detonation cycle time. In addition, detailed in-situ measurements with high spatio-temporal resolution have been relatively limited in RDCs thus far, particularly for liquid-based systems.

The extent to which RDCs will continue to be improved relies on a better understanding of the injector, detonation, and loss processes. In an RDC, there are relatively few studies that directly visualize or measure with spatial and temporal resolution the injector behavior and detonation structure and dynamics. The current study reports on ultra-high-speed (up to megahertz rates) planar laser-induced imaging to elucidate key detonation processes, including the unsteady liquid fuel injection dynamics in the presence of rotating detonation waves.

EXPERIMENTAL SETUP

Annular Rotating Detonation Combustor

A wide range of megahertz-rate, laser-based imaging diagnostics were performed in an annular RDC [ref]. The RDC geometry and its general operation have been described in previous works [19], and a brief description is provided here for reference. A schematic cross-section of the optically accessible RDC is shown in Figure 1. A 20 mm thick quartz outer body with an inner diameter of 136 mm serves as the outer wall for the annular detonation channel with a radial passage width of 10.7 mm. Air enters from a plenum through an annular converging diverging section with a throat gap of 1.42 mm. Immediately downstream of the air throat, gaseous hydrogen fuel is injected radially outward through 100 equally spaced orifices. The injector flow channel at first expands (at 10 deg.) leading into the combustor channel and finally fully expands into the combustor with a backward facing step (BFS). The detonation channel length is 90 mm (from BFS to combustor exit). Ignition is initiated by an O_2-H_2 pre-detonator originating from the centerbody.

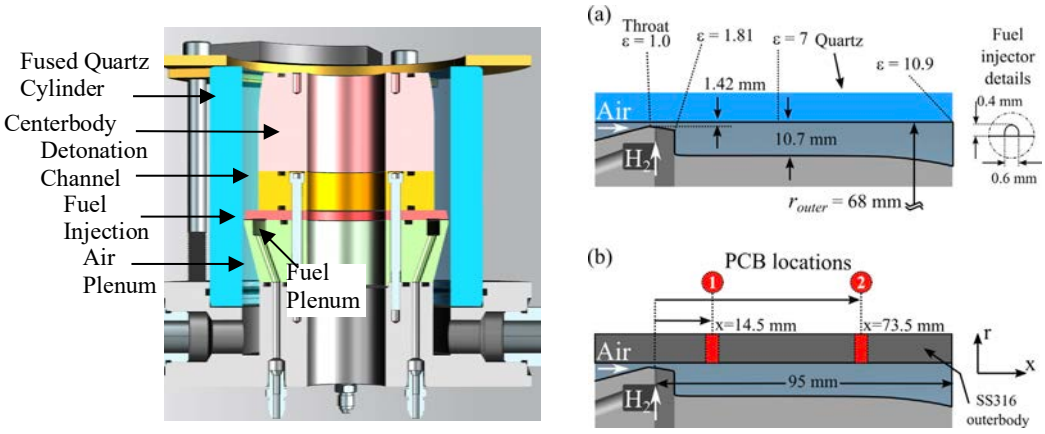

Figure 1. Cross-sectional schematics of the air-breathing annular RDC.

Linear Rotating Detonation Combustor

The linear RDC was used to perform up to 200 kHz imaging of the fuel mixing. Experiments were performed in the linear detonation combustor illustrated in Figure 2. A detailed discussion of the design and self- excited behavior of the test article is presented in [31]. A channel measuring 7.62 mm wide, 91 mm high, and 610 mm long forms the combustion chamber. Gaseous supplies of oxygen and natural gas are injected in the +*x* direction from the injector. The top of the chamber and the +*y* exit boundary are open to ambient conditions. The *y = 0* boundary is enclosed by a stainless steel plate which provides a mounting location for the ignition device.

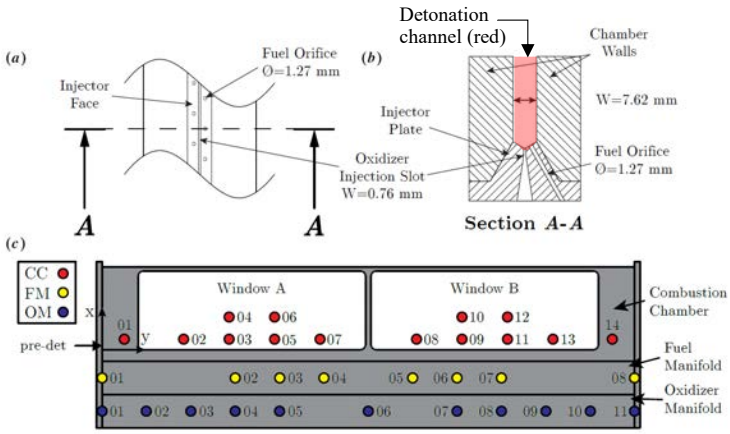

Figure 2. Schematics and layout for the Linear RDC.

The oxidizer injector consists of a 0.76 mm wide slot that spans the (*y* -direction) length of the chamber and is centered between the chamber walls. The fuel injection scheme incorporates 1.27 mm diameter orifices, distributed on alternating sides of the oxidizer slot along the full length of the combustion chamber. Each fuel injector introduces fuel at an angle of 30 deg. relative to the + *x*-axis.

There is a fused quartz window (Window B in Figure 2) that provides flow field visualization. Instrumented metal blanks (low and high frequency pressure measurements) were installed in the Window A position on both sides of the channel with and quartz windows were installed in the Window B position on both sides, as shown in Fig. 1 (c). To initiate the combustion process, a spark-ignited O_2-H_2 pre-detonator is used as an ignition source at the y = 0 end after reactants reach a steady state in their respective manifolds. Following ignition, the unique chamber and manifold dynamics in the combustor create self-sustained detonation waves at a rate of 6–12 kHz (depending on combustor operating conditions) that propagate along the length of the combustor (y-direction).

RESULTS AND DISCUSSION

An array of laser-based imaging diagnostics has been performed in the RDE devices to explore diagnostic challenges in the harsh RDC environment as well as to capture RDC physics and loss processes. Each measurement campaign was supported by a high-energy, high-repetition-rate burst mode laser and emphasized a measurement that was spatially and temporally resolved, i.e. a laser-based imaging measurement that was performed between a 100 kHz and 2 MHz repetition rate. An overview of some of the different measurements performed in the RDCs will be presented, with citations providing a reference to recently published manuscripts that cover these in greater detail.

SURVEY OF RDE DIAGNOSTICS PORTFOLIO

LIQUID FUEL INJECTION IMAGING IN THE ANNULAR RDC

Diagnostic Setup

A single jet of liquid diesel fuel is injected into the annular RDC to approximate one-way coupling of the hydrogen-air rotating detonation waves with the liquid fuel jet. One of the hydrogen fuel injection sites is removed and replaced with the orifice for the liquid jet. As shown in Figure 3, this liquid fuel orifice is located

at the same azimuth location as the blocked hydrogen orifice and 4.1 mm axially downstream. The internal geometry of the liquid fuel injector is cylindrical, with an orifice exit diameter of 0.3 mm and a length-to-diameter ratio of 6. The liquid fuel orifice is fed by a 2 mm diameter plenum with a length of 13.7 mm. The mass flow rate of liquid fuel is calculated using an experimentally determined discharge coefficient (C_d) of 0.26 and a pressure measurement upstream of the injector.

High-speed imaging of the liquid diesel jet was performed using 355-nm planar laser-induced fluorescence (PLIF) imaging, as shown in Figure 3 (b). The use of diesel for PLIF has been reported for dynamic imaging of fuels sprays in internal combustion engine environments at rates up to 50 kHz without added tracers [20]. In the current work, the high-power burst mode Nd:YAG laser's frequency-tripled 355-nm output was used to excite the diesel fuel in the detonation channel. The laser was operated at repetition rates up to 1 MHz with burst lengths up to 10 ms. The 10-ms burst duration provides PLIF imaging of approximately 40 sequential detonation periods for a test. The 355 nm output energy ranged from approximately 0.4–4.5 mJ/pulse. A laser sheet was formed using cylindrical and spherical sheet forming optics, resulting in a ~3 mm sheet thickness in the detonation channel. The laser sheet azimuthal location is centered on the liquid fuel orifice.

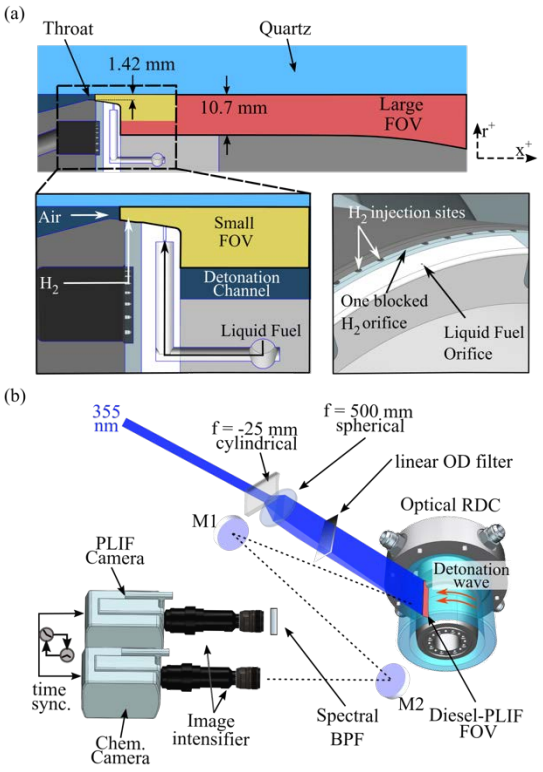

Figure 3. (a) RDC cross-section views showing the detonation channel, with enhanced injector views showing the liquid fuel injector. (b) Laser and optical arrangement for the PLIF and chemiluminescence imaging.

Multiple imaging schemes were implemented and explored to capture small-scale and large-scale fuel spray characteristics. Large field of view (FOV) schemes covered approximately the entire axial (x) length of the detonation channel. For this, the diesel PLIF used a highspeed Phantom v2012 camera paired with a highspeed image intensifier (Lambert, HiCatt), a 85 mm $f/1.8$ visible camera lens, a 420 nm longpass optical filter, and used a 40 ns exposure. Smaller FOV schemes typically operated at repetition rates of up to 1 MHz. Depending on the exact repetition rate and FOV, either an ultra-high-speed Shimadzu HPV-X2 camera or a Phantom TMX 7510 camera was used. Both cameras were typically paired with a 200 mm $f/4$ lens, a 420 nm longpass optical filter, and a 100 ns camera exposure. Due to the relatively dense spray in this region, the PLIF signal was sufficient to not need the use of an image intensifier for the 1 MHz imaging.

For all FOV schemes, broadband chemiluminescence imaging is typically performed simultaneous with the PLIF imaging, utilizing a Phantom v2012 camera, a high-speed UV intensifier (LaVision IRO), a 105 mm UV $f/4.5$ camera lens, and a 100 ns exposure. The PLIF measurements are made on the radial-axial (r-x) plane of the detonation channel. The chemiluminescence view is of a tangential plane (θ-x) that is centered on and perpendicular to the PLIF plane.

Global Fuel Spray Refill Characteristics

Figure 4 shows a complete detonation period with the arrival of the detonation wave near the beginning and end of the sequence encompassing ~250 μs. At 0 and 5 μs, prior to the detonation wave arrival, the spatial distribution of the liquid fuel spray within the injector and detonation channel is shown. During this quasi-steady state refill, the injection near field liquid centerline is expected to match closely with a canonical liquid-jet in supersonic crossflow. For x < 30 mm, the spray is confined towards the outer radius

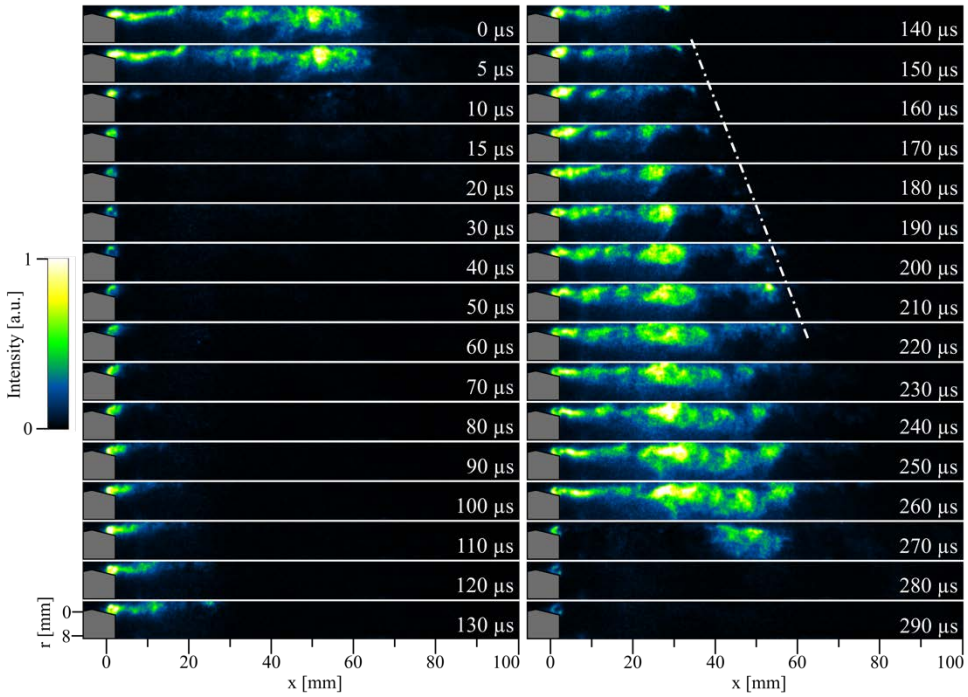

Figure 4. Image sequence of diesel PLIF (large FOV, 200 kHz) across one period of the detonation wave passage. The first 5 frames are spaced 5 µs apart and the remaining frames are spaced by 10 µs.

of the channel, and for x > 30 mm the spray expands to fill much of the channel's radial width. This spatial distribution closely follows the mixture evolution of a gas-gas supersonic jet entering the same channel geometry under the same flow conditions [19, 21], indicating that the spray is entrained into and convected downstream by the supersonic air crossflow.

At 10 µs, the detonation wave arrives at the PLIF plane causing a complete extinction of the PLIF signal in the channel. While detonation-induced spray breakup is expected, the nearly instantaneous extinction of the signal also suggests that the bulk of the liquid droplets may be shifted out of the PLIF measurement plane due to detonation-induced azimuth momentum. Hence, fuel PLIF in the near field would indicate fresh injection into the channel. Between ~10–60 µs, the fuel spray appears to have a dwell time or recovery period, during which the fuel spray is not admitted into the channel. Between 15–70 µs, the PLIF signal at the liquid injection site begins to monotonically increase, suggesting the liquid injector is recovering. At ~ 70 µs, the liquid column is observed to propagate into the chamber, marking the admission of fuel into the axial length of channel. This axial transport of reactants into the channel appear to be primarily attributed to the air-stream recovery, since the liquid jet momentum exiting the liquid orifice is initially fully radial.

Between 80–260 µs, the air stream advects the fuel spray further into the detonation channel. During the fuel spray recovery process, very little diesel is observed in the recirculation zone downstream of the BFS suggesting low entrainment strength. The fuel spray spatial distribution shows a gradual radial spread during the refill process until detonation wave arrival at ~270 µs.

Fuel spray injection nearfield characteristics

The upper panel of Figure 5 shows a 1 MHz diesel PLIF image sequence of the near field fuel spray during the detonation wave arrival, with the lower panel extending the time sequence in increments of 3 µs. The orange lines qualitatively represent the boundary of the spray. Before detonation wave arrival the near-field spray is mostly confined to the outer radius of the channel. After ~3 µs, the majority of the fuel spray is removed up to the BFS. Later in time, the air inflow is unable to force the core of the liquid jet axially downstream, and between 18–24 µs the fuel spray is primarily propagating in the radially positive direction.

By 30–36 μs, the fuel spray trajectory begins to tilt downstream, indicating that the air crossflow is beginning to recover. Similar to many other of the cases considered, the spray is not observed axially upstream of the liquid jet orifice site. Moreover, feature tracking of the PLIF images suggests that the orifice is not turned off in response to the detonation wave passage and continues to flow liquid fuel into the channel, albeit at a temporarily much slower rate.

It is of interest to measure the fuel spray trajectory emanating from the liquid orifice as this affects the penetration into the air crossflow and subsequent mixing and dispersion across the detonation channel. The spray trajectory is determined by tracking the spray windward leading edge, performed by determining the location where signal intensity decays to 25% of the maximum for every axial (x) location. This calculation is then repeated at each time instance. Figure 6 shows the average trajectory (calculated using 40 consecutive detonation periods) immediately prior to the detonation wave arrival. For reference, a steady-state model (Equation 1) for a transverse liquid jet injected into a supersonic crossflow is compared, [23]

$$y/d_j = 4.73q^{0.3}(x/d_j)^{0.3} \quad (1)$$

where q is the momentum flux ratio between the air and the liquid fuel, d_j is the liquid orifice diameter, and x and y are the axial and radial trajectory coordinates, respectively. As q increases, the near field fuel spray penetration height increases, as expected. The fuel spray trajectories show reasonable agreement with the steady-state model up to ~10 d_j. Beyond ~10d_j, the spray penetration is lower as compared to the model, correlating with the location of the large area change entering the detonation channel. As q and the penetration height decrease, the fuel spray is entrained into the shear layer formed between the incoming fresh reactants and the wake formed behind the BFS. While the empirical correlation was developed for steady flow, it's quite surprising that the dynamic variations in q still result in reasonable agreement. This highlights that (a) a steady trajectory correlation may be appropriate to predict fuel jet penetration once the injector reasonably recovers with in a detonation period and (b) the fuel spray has recovered to a nominal/reasonable "steady" position within the few hundred microseconds of the detonation period. The sprays reduced penetration, though, may highlight that the liquid jet is only quasi-steady state for these relatively small timescale detonation periods, a topic considered further in the next section.

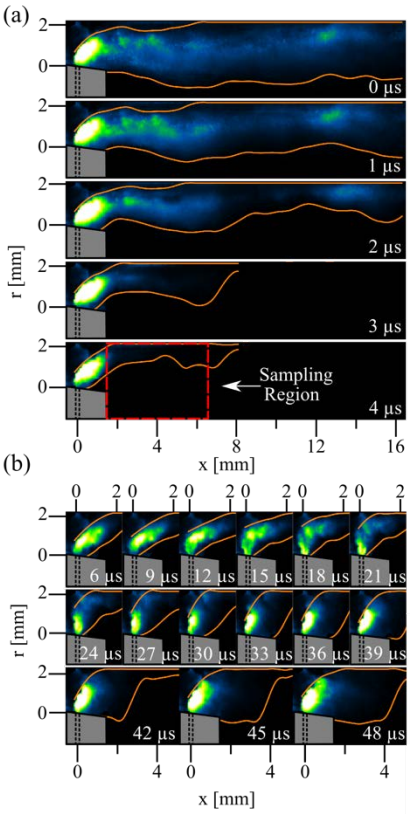

Figure 5. Diesel PLIF image sequence from the smaller FOV at 1 MHz for Case 1. Upper and lower panels are from the same image sequence with different time increments. Red box is the sampling window in the refill analysis.

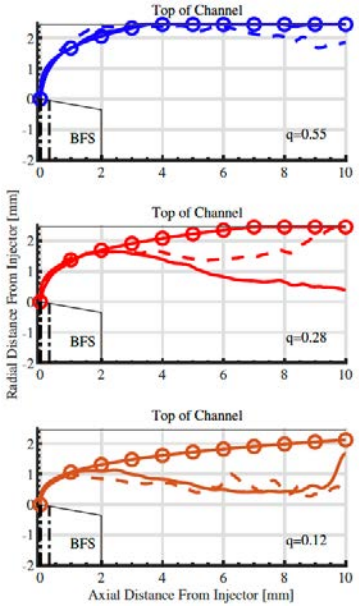

Figure 6. Experimental penetration (solid and dashed lines) compared to empirical correlation (circles, Eqn. 1) for various momentum flux ratios. Solid and dashed lines correspond to air mass flow rates of 0.46 and 0.23 kg/s, respectively.

Fuel Spray Dwell Time Quantification and Modeling

The transient nature of the reactant refill process and the initial purely radial liquid injection motivates clarity on the recovery time or dwell time definition. While the liquid jet may be admitting

fuel radially, due to fast recovery from larger pressure drops across the liquid fuel injector, the axial motion of this liquid plays an important role in the spray development, thereby affecting detonation characteristics. Hence, the beginning of the refill quantification should be dependent on the axial liquid penetration after the passage of the detonation wave.

To quantify the 'dwell time', pixel intensity values were averaged in a 5.1 mm (x) × 5.1 mm (r) region, immediately downstream of the BFS (see Figure 5 at 4 μs). After the detonation wave passage, the average signal in the box drops. During the liquid axial reissue phase, when the signal in the box reaches 10% above the background signal, the spray refill for that cycle is assumed to have begun and the time period leading up to that point is the fuel injector 'dwell time'.

The dwell time variation across the tested RDC operating conditions is shown in Figure 7. For greater statistical confidence, several test cases were repeated at the same RDC operating condition. Figure 7 (a) shows the variation in dwell time (as a percentage of the detonation period) versus the air to liquid fuel momentum flux ratio for two different air mass flow rate RDC cases. Readily observable is the fact that the 0.23 kg/s test cases generally have a higher refill cycle fraction of 40% compared to the 0.46 kg/s test case which is 20%. This suggests that the air momentum plays a significant role in the RDC recovery time, an expected result (since as a first-order effect, the air injector is less stiff for a lower air mass flow and hence is anticipated to take longer carry the liquid fuel axially into the detonation channel). As shown in Figure 7 (a) there appears to be no trend with increasing q for the 0.23 kg/s test cases and a decreasing refill time for the 0.46 kg/s test case. This suggests that dominant parameters such as air momentum and total flow rate might play a larger role in refill characteristics.

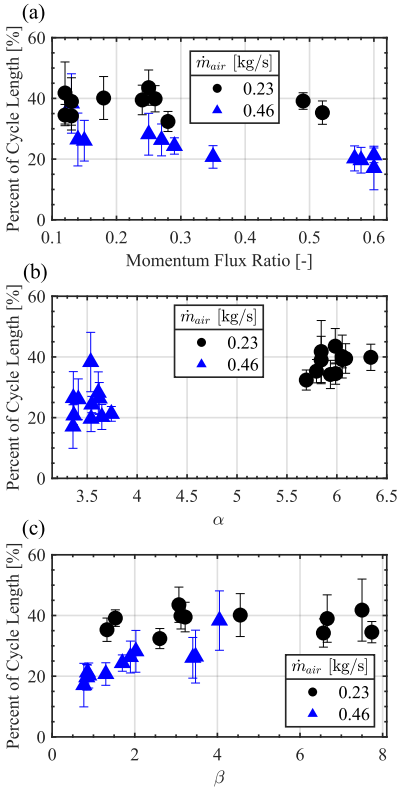

Figure 7. Fuel spray dwell time as a function of (a) momentum flux ratio, (b) α, and (c) β. The bars represent ±1σ.

We hypothesize that the dominant factors influencing the liquid injector response are the detonation impulse strength and the pressure drops across the air and liquid fuel injector. The dominant parameters hypothesized can be reduced into the following (a) detonation peak pressure (Ppeak), (b) air-injection pressure (Pox.pl.), (c) mean chamber channel pressure (Pmean), and (d) liquid injector plenum pressure (PLFinj). The increase in detonation peak can cause an increased adverse pressure gradient which can lead to longer refill times. However, increase in ΔPair = Pox.pl − Pmean or ΔPLF = Pox.pl − Pmean can lead to a reduction in refill times due to greater air or liquid fuel momentum. Combining these parameters based on the proportionality, we propose the following condensed parameters Ppeak/Pox.pl −Pmean and Ppeak/PLF −Pmean. Plotting the refill times against these two condensed parameters in Fig. 8(a) and (b) respectively shows linear trends with increasing parameter. Thus statistical analysis provides two useful condensed parameters that can be used in designing liquid injectors in RDCs.

MEGAHERTZ OH-PLIF IMAGING IN THE ANNULAR RDC

Diagnostic Setup

A custom high-energy, high-repetition-rate, nanosecond burst-mode Nd:YAG laser (Spectral Energies) was implemented in the Air-Hydrogen Annular RDE THOR. This system generated sequences of more than 150 ultraviolet pulses with 400 mJ/pulse at 1 MHz and 150 mJ/pulse at 2 MHz, uniquely enabling MHz-rate OH-PLIF imaging in the annular RDE. The experimental setup for performing the MHz-rate OH-PLIF

measurements in the RDC is shown in Figure 8. The OPO was tuned to a wavelength near 284 nm to excite the $Q_1(9)$ transition in the (1, 0) band of the OH $A^2\Sigma - X^2\Pi$ system. While this burst-mode laser/OPO system enables wide tunability in wavelength, the OH species was targeted because it is an important combustion species that shows the reaction zone locations (deflagration and detonation) as well as the locations of combustion products. This approach of OH-PLIF has advantages to conventional OH* chemiluminescence imaging since OH* imaging only shows the reaction zone locations but is a line-of-sight technique that integrates the light emission in the imaging direction.

For the MHz-rate demonstration, the non-premixed annular RDE was operated with ambient temperature air and hydrogen fuel. The entire outer body of the RDE is a transparent fused quartz cylinder providing optical access to the annular injection system and combustion channel. Once ignited, the detonation wave propagates in the azimuthal direction around the annulus, with a mean tangential velocity of ~1.5 km/s and a cycle frequency of ~4 kHz, corresponding to a period of ~ 250 μs.

Radial-Axial Plane MHz-rate OH-PLIF: The MHz OH-PLIF imaging system allows tracking of the flame reaction zone structure and combustion dynamics with high spatial and temporal resolution to elucidate the physics and chemistry of the RDE. Figure 9 shows a selected sequence of sixteen images (out of 150) from the 1 MHz OH-PLIF imaging. A brief summary of a few salient resolved features includes:

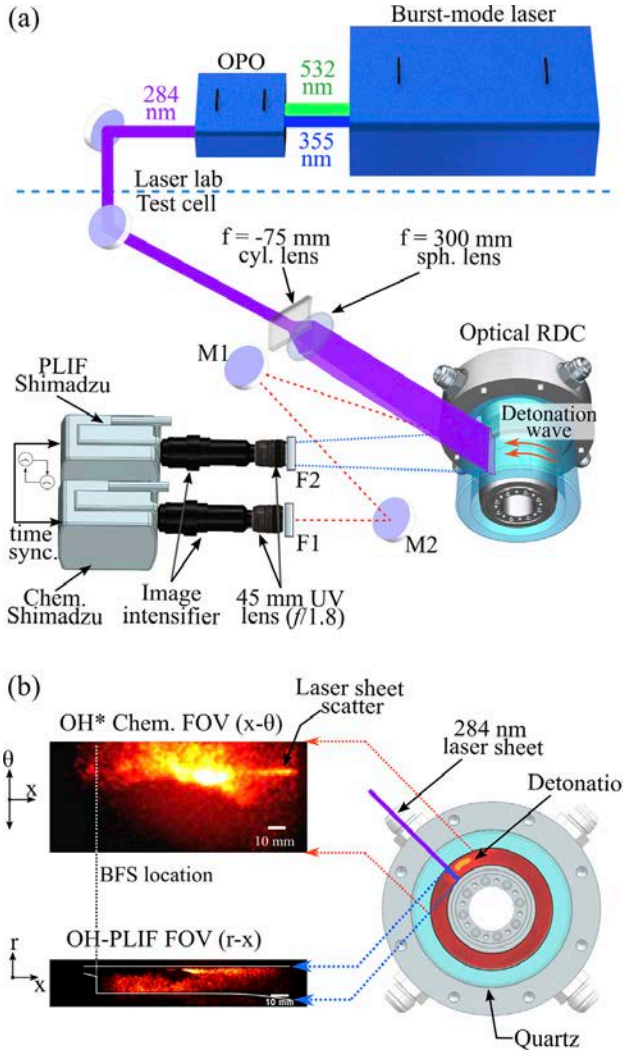

Figure 8. New burst-mode laser system optical layout (a) that was leveraged in the Phase-I to perform MHz-rate OH-PLIF imaging in an Air-H_2 annular RDE. Where (b) and (c) show the radial-axial and radial-azimuthal, respectively, OH-PLIF measurement planes investigated.

- **Recirculation zone:** The first image captures the air-fuel mixture refilling the combustor channel (37–42 μs), with Region 1 identifying a recirculation zone filled with combustion products (i.e., OH). The time evolution of Region 1 OH intensity suggests that the recirculation zone is a mixture of old products and new reactants.
- **Fresh fuel/air reactant refill**: Region 2 is an area devoid of OH and signifies the unreacted air-fuel mixture. The refill is radially and axially nonuniform.
- **Detonation propagation:** the detonation wave is observed to propagate non-uniformly through this radial-axial measurement plane, typically leading in Regions 1 and 3, where the mixture contains fresh air/fuel and hotter combustion products.
- **Deflagration:** the behavior of Region 3 (interface between the hotter previous cycle combustion products and new inflowing reactants) suggests this is a mixture of products and reactants. Low levels of deflagration appear to occur in Region 3. Moreover, after the detonation wave passage through the measurement plane, there are multiple islands devoid of OH (e.g. 47 μs solid circle), indicating unburned fuel behind the detonation wave. These islands typically convert to OH in a few microseconds, indicating deflagration behind the wave as the

unburned fuel is rapidly mixed out with the hotter combustion products.

- **Combustion products in injector**: OH is observed inside the injector soon after the passage of the detonation wave (e.g. 48 µs dashed circle). The temporal evolution of the OH signal suggests that this OH is convected from the channel annulus into the injector (due to the high pressures of the detonation wave and cessation of inflowing reactants from the momentary pressure gradient reversal).
- **OH-PLIF vs. OH* chemiluminescence imaging:** Figure 10 shows the different, but complementary information that OH-PLIF provides compared to OH*. OH* shows the general detonation behavior across a sector of the RDE annulus, however is path-integrated (predominantly in the radial direction), and only shows new reaction zone combustion. OH-PLIF provides spatial resolution of the flowfield, with the ability to resolve the radial, axial, and azimuthal directions; the OH-PLIF also captures combustion products, which OH* does not, thus providing additional details on the RDE physics.

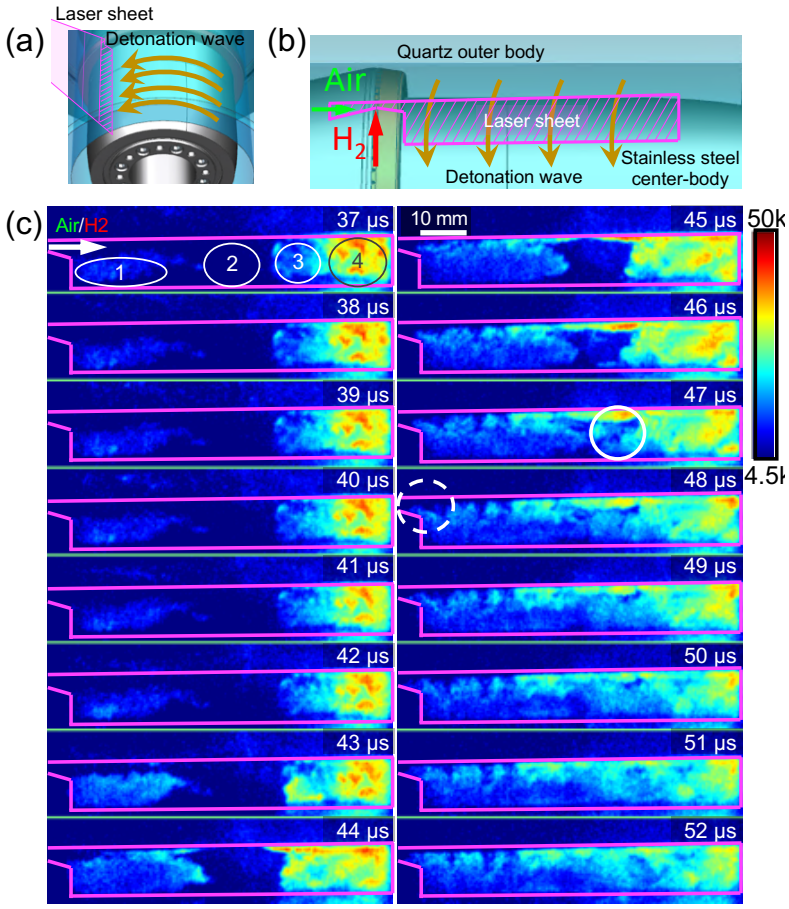

Figure 9. 1-MHz OH-PLIF imaging an annular RDE showing the variation of flame reaction zone structure. The color bar represents the relative OH signal in arbitrary units.

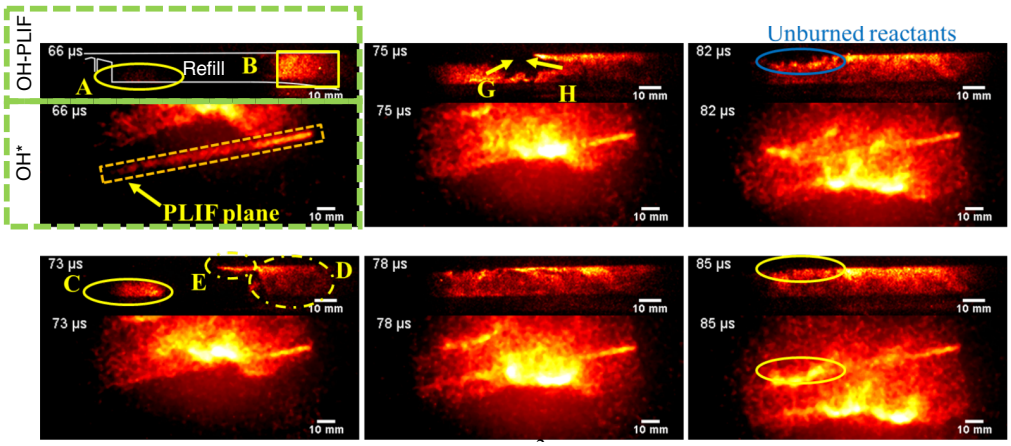

Figure 10. Simultaneous 1-MHz OH-PLIF and OH* imaging for six time instances showing the detonation wave behavior. The OH-PLIF is shown in the top of each image and the corresponding OH* is shown in the bottom. These images show the complementary information provided by OH-PLIF and OH*.

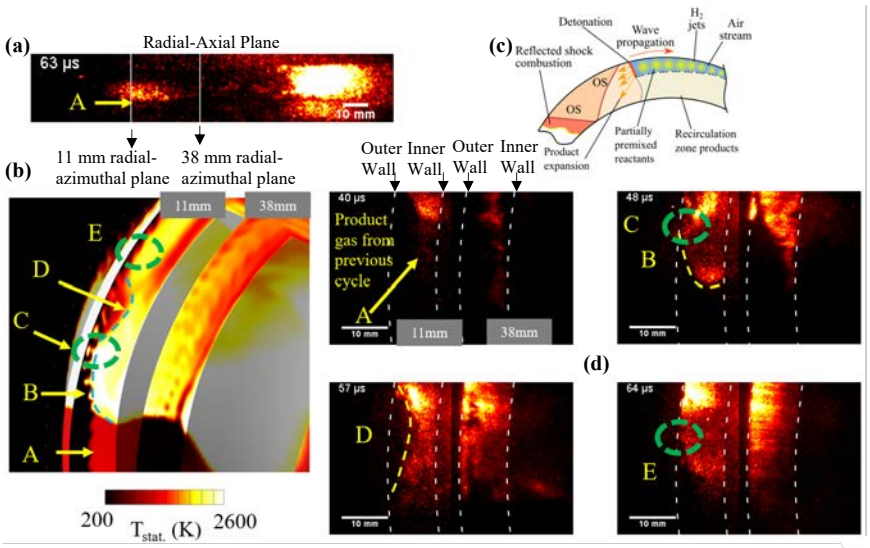

Figure 11. Simultaneous radial-azimuthal dual-plane OH-PLIF at 1 MHz rate in the annular RDE. (a) Radial-axial plane OH-PLIF showing locations of radial-azimuthal planes. (b) URANS simulation of the RDE. (c) Schematic of RDE processes inferred from the diagnostic measurements and URANS results. (d) Radial-azimuthal OH-PLIF planes at four time instances capturing the detonation propagation behavior.

Radial-Azimuthal Plane MHz-rate OH-PLIF: The non-uniform detonation wave propagation through the radial-axial measurement plane, combined with the inherent three-dimensionality of the RDE flowfield, motivated the investigation and extension of OH-PLIF in the radial-azimuthal plane. Additionally, to investigate the extension of the single plane OH-PLIF to a multiple-plane OH-PLIF for more accurately resolving the instantaneous 3D combustion structure, OH-PLIF was extended to simultaneous dual-plane radial-azimuthal measurement planes. For this, the 1 MHz OH-PLIF laser pulses were split and formed into two parallel thin laser light sheets. A brief summary of a few features from this perspective includes:

- **Reactant refill radial dependence:** The simultaneous dual plane OH-PLIF measurements confirm and further characterize the azimuthal structure of the reactant refill regions as inferred from the lack of OH.
- **Non-uniform leading detonation wave front:** Figure 11 at 40 µs shows that the detonation wave front leads in the recirculation zone region containing hot products from the previous cycle.
- **Trailing shocks and shocked induced combustion:** The radial-azimuthal planes provide the radial structure of unburned fuel pockets near the outer wall quickly followed by rapid combustion.
- **RDE physics:** The radial-azimuthal OH-PLIF measurements complement the radial-axial OH-PLIF and the path-integrated OH* chemiluminescence. Combined with URANS simulations (e.g. Figure 11b), these enable a more complete picture of the RDE physics, shown schematically in Figure 11c. This shows that there is a shock system trailing the dominant detonation wave front, causing rapid shock induced combustion a few microseconds later.

2-MHz OH-PLIF: The OH-PLIF was investigated and demonstrated up to a 2 MHz imaging rate in the RDE. This provides an unprecedented time resolution of the propagating detonation front. Figure 12 compares two sequential frames of the leading detonation wave front comparing the laser system operating at 500 kHz, 1 MHz, and 2 MHz OH-PLIF rates. The 1–2 MHz rates are necessary to resolve the fine scale details of the propagating wave fronts reactant consumption and subsequent unburned pocket evolution.

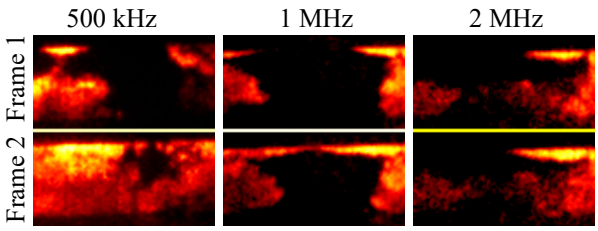

Figure 12. Two sequential OH-PLIF images acquired using a 500 kHz, 1 MHz, and 2 MHz OH-PLIF imaging (radial-axial) of the RDE at similar phases of the detonation wave passage through the imaging plane.

TIME-RESOLVED AIR INJECTOR VISUALIZATION IN THE ANNULAR RDC

Results from the liquid fuel spray and OH-PLIF measurements indicate that the steady state momentum flux ratio is not the sole parameter of influence for the recovery behavior of the liquid jet. The oxidizer transient recovery characteristics also plays a major role in the jet penetration into the chamber. Several burst-mode laser diagnostic options were considered and explored to spatially and temporally capture the oxidizer response and recovery characteristics near the fuel injection, upstream into the oxidizer plenum, and further down inside the detonation channel. For all reported air injector visualization, the laser beam path, sheet forming optics, camera set up, and camera FOV is shown in Figure 13.

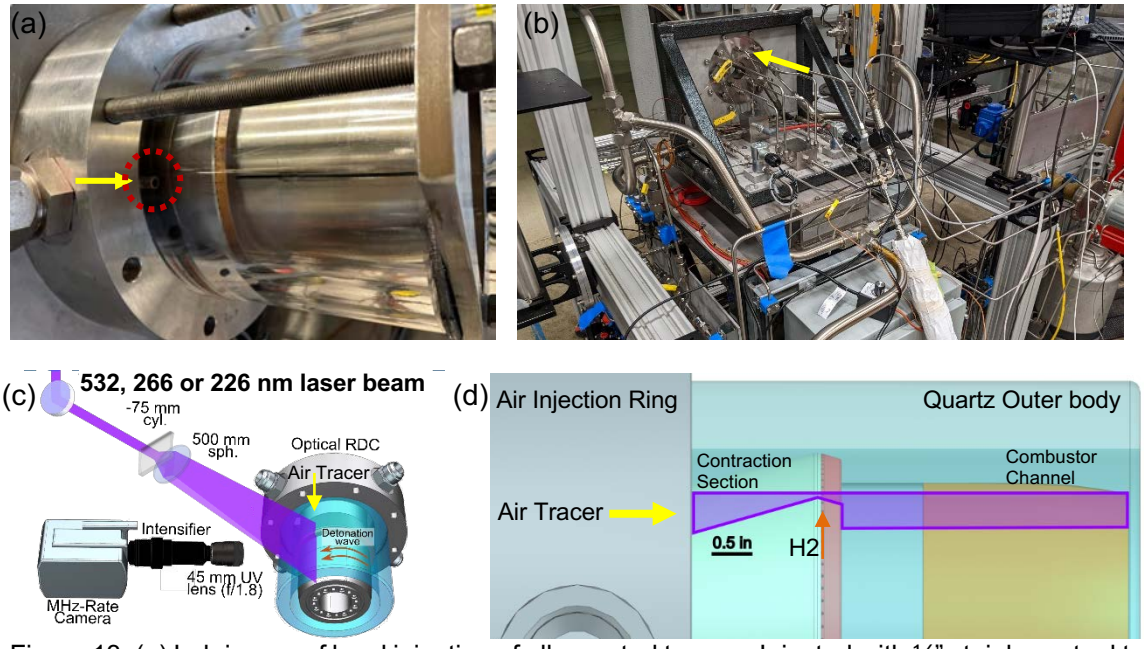

Figure 13. (a) Lab image of local injection of all reported tracers. Injected with ¼" stainless steel tube circled in red outline (b) Back end of RDE showing injection of air tracer as yellow arrow (c) Experimental set up for testing air tracers for each laser wavelength. (d) Camera FOV and laser sheet location to view that contraction section and complete combustor channel

The diagnostic choices that were selected had to satisfy the following conditions:

- The oxidizer visualization technique must allow for simultaneous liquid PLIF diagnostics
- The visualization technique should have minimal influence on the thermochemistry of the oxidizer.
- The technique must use laser excitation wavelengths that has the following spectral characteristics

    - The excitation wavelength should not excite the liquid fuel jet. This requirement eliminated the use of UV diagnostics due to the large spectral absorption bandwidth of diesel fuel (200 – 360 nm)
    - The emission spectral bandwidth must be spectrally or temporally separated from the liquid PLIF signal.[i]
    - The emission spectrum must also not overlap with the OH* chemiluminescence emission from the flame front or must be appropriately temporally gated
- Minimal participation of liquid jet in the visualization of the air-recovery.
- The oxidizer PLIF tracer should have sufficiently low Stokes number to faithfully follow the flow. This requirement poses an upper limit on a tracer particle size and particle density due to high-speed inlet of the oxidizer stream.

Table 1: Comparison of some of the air visualization techniques demonstrated in the annular RDC

TRACER	PHASE	WAVELENGTH (NM)	VIABILITY?	NOTES
EOSIN Y DYE PARTICLES	SOLID	532 ABSORPTION	NOT VIABLE	LOW SNR
OIL SCATTERING	LIQUID	532 SCATTERING	NOT VIABLE	LOW SNR AND OIL STICKING TO SURFACES
EXTRA VIRGIN OLIVE OIL (EVOO)	LIQUID	532 PLIF	NOT VIABLE	LOW PLIF EFFICIENCY REQUIRING HIGH 532 NM ENERGIES
NITRIC OXIDE (NO)	GAS	226 PLIF	LOW VIABILITY	SIGNAL QUENCHES WITH AIR. REQUIRES OPTICAL PARAMETRIC OSCILLATOR (OPO). MORE BENEFICIAL FOR GASEOUS INJECTOR STUDIES
NITROGEN DIOXIDE (NO2)	GAS	532 PLIF	LOW VIABILITY	LOW PLIF EFFICIENCY, RESULTING IN BRIGHT SURFACE AND QUARTZ FLUORESCENCE
BIACETYL	GAS	355 PLIF	VIABLE	MEDIUM SNR. EFFICIENT WAVELENGTH GENERATION. DISTURBS LOCAL FLAME CHEMISTRY. DIFFICULT TO CLEAN.
ACETONE	GAS	266 PLIF	VIABLE	HIGH SNR. EFFICIENT WAVELENGTH GENERATION. DISTURBS LOCAL FLAME CHEMISTRY

To satisfy the requirements mentioned above, the optimal laser excitation wavelength is 532 nm and the particle size had to be < ~1 μm to meet the Stokes criterion for the air-stream visualization (speeds up to Mach 2). The 532 nm can be generated at high repetition rates and large energy/pulse with the Nd:YAG pulse burst laser systems. Towards that goal, the following diagnostics were considered for air-stream recovery characterization:

- Oil seeding PLIF – using extra virgin olive oil (EVOO) PLIF.
    - Sub-micron droplets will be introduced into the airstream at the azimuth location of the PLIF laser sheet.
    - The EVOO PLIF has a 532 nm excitation wavelength and emission wavelength in the 600 nm range.[ii]
- Dry tracer seeding – Eosin Y dye powder (excitation at 532 nm) and emission at 580+ nm.
- Particle seeding for flow visualization of pure air-stream recovery (no liquid jet) to obtain time uncorrelated data of the air-recovery at a given operating condition.
- Introduction of gaseous tracer – NO2- which has an excitation wavelength at 532 nm.

The solid and liquid PLIF tracers demonstrated in the RDC were observed to not appropriately fill the flow field, not faithfully track the flow, and would adhere to the inner and outer body walls, causing significant background measurement challenges. Based on these observations, gaseous tracers became the most promising solution.

100 kHz NO-PLIF

Nitric Oxide (NO) PLIF is a well-studied tracer technique, such as visualizing boundary layers. NO is an attractive species as it minimizes affecting the combustion chemistry, only requires a small amount of deep ultraviolet (UV) energy centered at 226 nm, and the fluorescence emission is in the range of 240-300 nm, which is the range of UV intensifiers. Therefore, NO PLIF of the air stream combined with 355-nm of the fuel spray would be a good combination to simultaneously visualize both propellant streams. To generate the 226 nm, a nanosecond KTP OPO was pumped with 532 and 266 nm from a burst mode laser. The beam was sent into the RDC as shown in Figure 13c and the sheet illuminated the combustor as shown in Figure 13d. Figure 14 shows a representative time sequence of the NO-PLIF in the annular RDC. The signal to noise ratio was observed to be low due to the low NO concentration in the contraction section and into the combustor channel. However, just beyond the air throat and after the fuel injection, the NO PLIF is visible. In this case, the air recovery time was measured to be around 50 μs. The variation in PLIF signal is believed to be due partly to the pressure variation across the subsonic to supersonic injector. If repeated, a more pressure insensitive NO line may improve the PLIF signal.

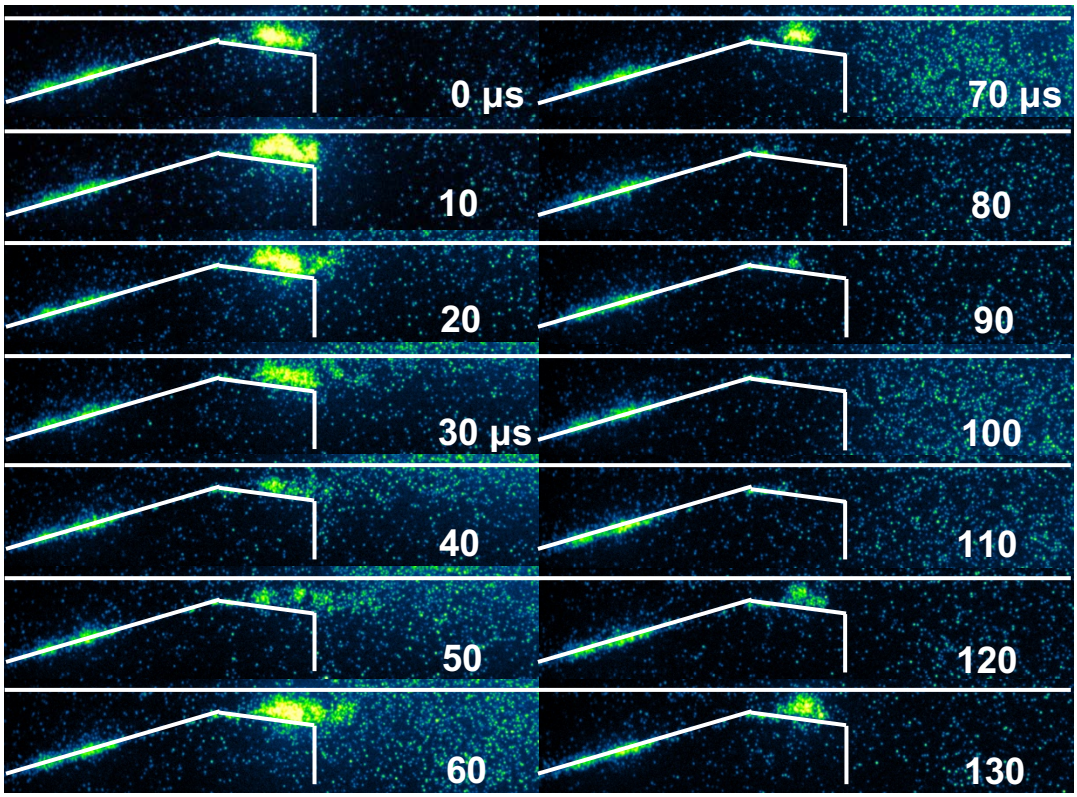

Figure 14. 10,000 ppm NO in N_2 is injected/traced to perform 100 kHz NO-PLIF to visualize air recovery time after the detonation wave passage, approximately 50 µs for this condition. Low NO concentration and pressure variation in the combustor as the air spreads in the azimuthal location results in low signal to noise ratio

NO_2-PLIF

NO_2-PLIF was a promising technique that would allow for 532 nm excitation and emission spectra around 600-700 nm. However, we observed low signal levels, believed to be due to the low NO_2 fluorescence efficiency. Approximately 120 mJ/pulse at 532 nm was required to fluoresce a 1.5" axial-length sheet. At these energies the quartz and center body risked being damaged. In addition, strong stray laser light reflections and ablations were difficult to filter out, as shown in Figure 15, despite the image collection system having 3 x 532 notch filters (OD 12 total) and 1 x 540 nm long pass filter (OD 7).

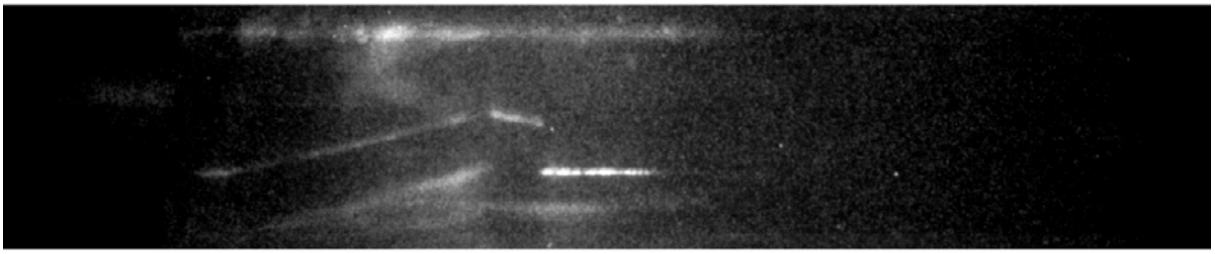

Figure 15. Image with no intensifier gain showing the 532 nm generate intense illumination of the RDC quartz and center body causing heightened background around the injector areas of interest.

The next attempted air tracers in the RDC were biacetyl and acetone. Figure 16 compares low-speed, facility camera images of their effects the overall RDC exhaust flow. Comparing the detonation wave speed and frequency shows little difference with addition of small amounts of these tracers, though.

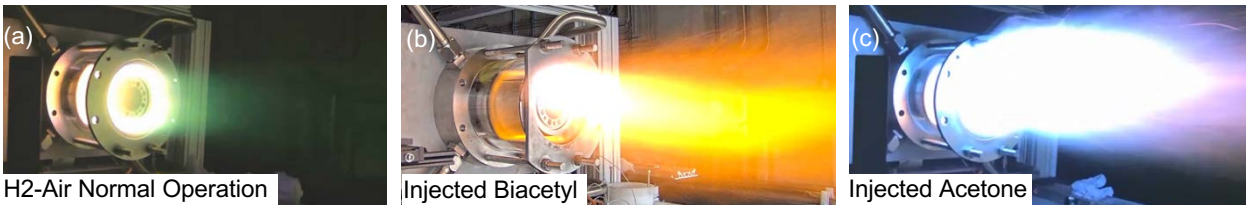

Figure 16. THOR – (a) Low speed image of H2-Air normal operation with either (b) local biacetyl tracing or (c) local acetone tracing

100 kHz full combustor and 200 kHz zoomed in Acetone-PLIF

Acetone was heated to build vapor pressures of 220-350 psi in a sampling cylinder and injected into the air plenum in the same configuration that is shown in Figure 13. Acetone PLIF is a well studied technique with high SNR and uses 266 nm for fluorescence and emits 420-500 nm. The first round of acetone PLIF was completed with 8 mJ/pulse at 100 kHz for a 4.5 ms burst duration. The PLIF was imaged with a high speed Phantom v2012 coupled with a Lambert HiCATT intensifier with an 85 mm F/1.4 lens which resulted in a 3.6 px/mm resolution. A 439 ± 139 nm bandpass and 266 LP were used to minimize background chemiluminescence and 266 scattering. The intensifier gate was set to 50 ns and the laser pulse width was 7 ns.

Figure 17 shows examples of acetone PLIF for visualizing the injector air stream in the RDC. The blue elipses show the air contracting before the injector throat and its noticed that the air is not consistently filling

the contraction section volume. Lastly, the air can be tracked into the combustor channel, which allows for air recovery meausurements.

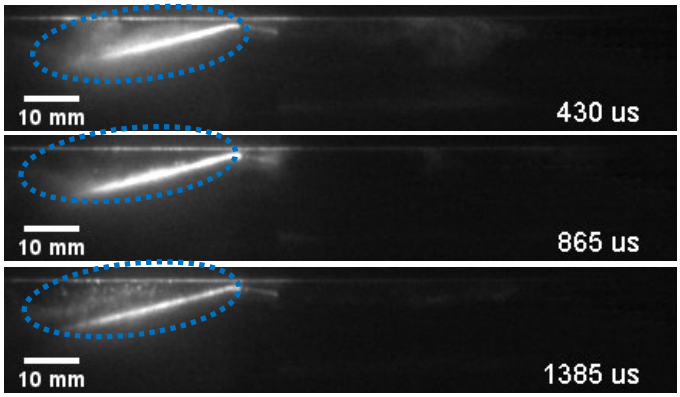

Figure 17. Three instantaneous acetone PLIF images from local tracing of acetone.

Figure 18 shows acetone PLIF image sequences of one detonation wave passage that shows and air recovery time of under 20 µs. Figure 19 shows acetone PLIF visualization where the field of view now includes more of the detonation channel. The increase in speed to 200 kHz resulted in a lower 266 energy of 5 mJ/pulse. The PLIF was imaged with a high speed Phantom v2012 coupled with a Lambert HiCATT intensifier with an 85 mm F/1.4 lens in a 6.8 px/mm resolution. A 439 ± 139 nm bandpass, 266 LP, and a 532 notch were used, because some 532 was . The intensifier gate remained the same at 50 ns and the laser pulse width was 7 ns. Saturation is seen just past the throat due to the high concentration of Acetone.

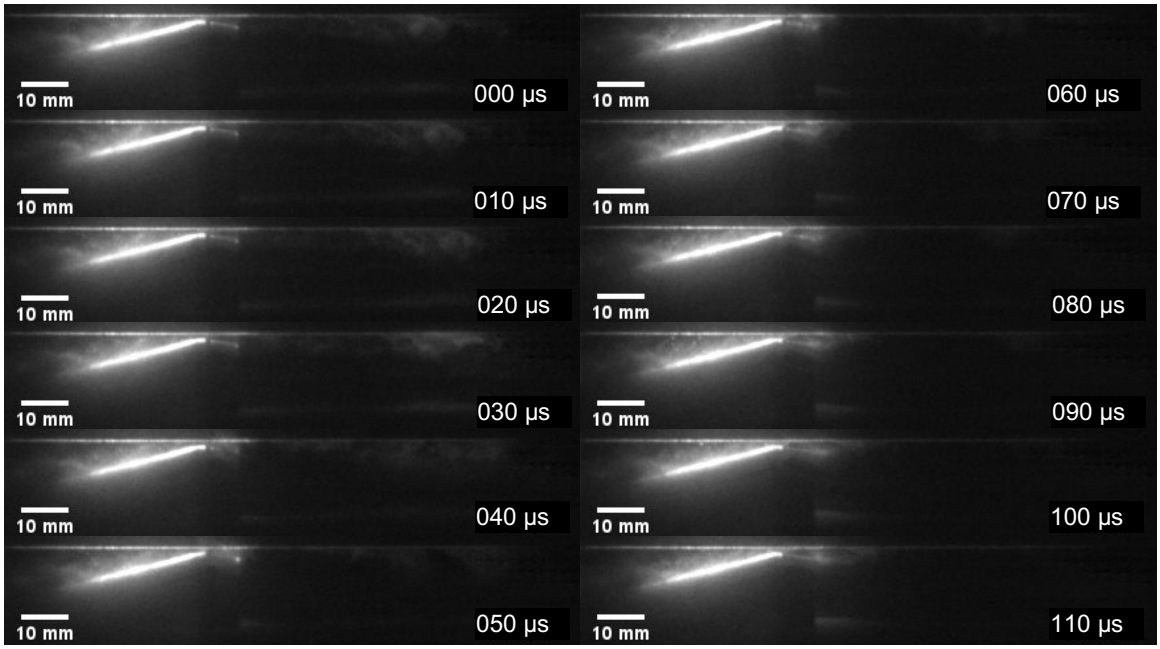

Figure 18. 100 kHz Acetone PLIF of detonation wave pass at 40 µs to show air recovery time of under 20 µs to recovery and 50 µs to penetrate 15 mm into the combustor channel

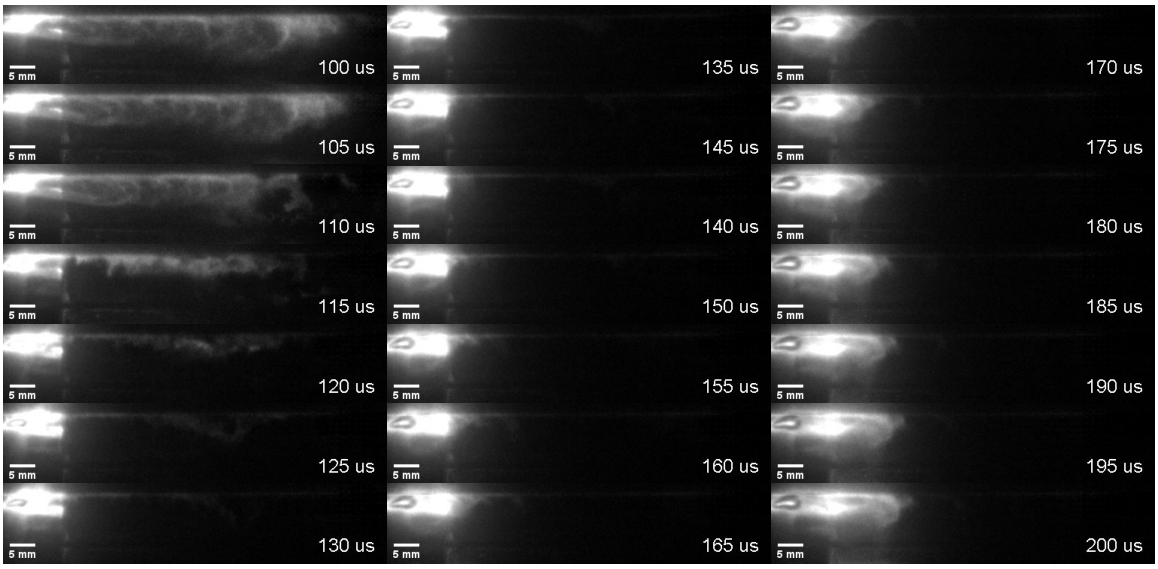

Figure 19. 200 kHz Acetone PLIF of detonation wave pass at 115-130 μs to show air recovery time of under 20 μs

FUEL MIXING PLIF IMAGING IN THE LINEAR RDC

Diagnostic Setup

Multiple different laser sheet orientations were implemented to investigate diagnostic extension to capturing the three-dimensional mixing field in the linear RDC. An overview of the optical setup and mixing measurement plane orientations is shown in Figure 20. A Spectral Energies Nd:YAG burst-mode laser was used as the excitation source, and was frequency quadrupled to produce 12-ns 266-nm pulses at 100–200 kHz repetition rates. Figure 20(e) provides a schematic of the optical layout. For vertical (X-Y) plane PLIF, a single laser sheet was utilized. A Phantom v2012 high-speed CMOS camera was coupled to a Lambert HiCatt intensifier (GaAsP photocathode) and equipped with a Nikon 200 mm f/8 visible lens for acetone PLIF imaging. A bandpass filter (Semrock FF01-439/154) was used to isolate the acetone fluorescence and to reduce flame luminosity. An additional 266 nm longpass filter (Edmund Optics #12-255) was installed to prevent the intensifier from capturing scattered laser light. The intensifier gate was set to 20 ns to improve temporal resolution and reduce background chemiluminescence signals. For the X-Y acetone PLIF imaging, the camera spatial resolution after a dot target calibration was 0.095 mm per pixel. For the Y-Z acetone PLIF, it was 0.172 mm per pixel.

To evaluate the feasibility of multiple-plane acetone PLIF for the three-dimensional mixing field and to provide further insight into the physics of the Linear RDE, 100 kHz acetone PLIF on two simultaneous Y-Z planes in the Linear RDE (shown in Figure 20) was designed and demonstrated. A key innovation here is the two planes of simultaneous PLIF using a single intensified camera for imaging. For this Y-Z (horizontal plane) acetone PLIF, two laser sheets, each measuring 540 μm thick and 7.6 mm wide, were formed in the Y-Z plane using similar optics as in the X-Y (vertical plane) measurements. With a reduced sheet size, the laser fluence increased significantly, and thus a longer laser burst duration of 2.5 ms was implemented. The laser and imaging equipment remained the same as for the X-Y plane measurements, although the PLIF camera was raised above the test article and the viewing mirror was tilted downward to give the camera a vantage from which to view both of the laser sheets. A spatial calibration was implemented to correct raw images such that a top-down view on the Y-Z plane was obtained. A single image calibration transformation matrix was needed as the final laser mirror and the PLIF camera were placed on vertical translation stages which traversed the X-direction in a synchronized manner.

For each dual-plane measurement, the two parallel Y-Z planes were spaced by 12.7 mm. The X position of the dual-plane PLIF was then progressed away from the injector face, resulting in a total of nine Y-Z planes of 100 kHz acetone PLIF. The X positions of the nine Y-Z planes include 3.18 mm, 6.35 mm, 9.52 mm, 12.70 mm, 15.88 mm, 19.05 mm, 22.22 mm, 25.40 mm, and 28.58 mm. Much of the analysis focuses on four of these planes, labeled HP1 (at X = 6.35 mm), HP2 (at X = 12.70 mm), HP3 (at X = 19.05 mm), and HP4 (at X = 25.04 mm).

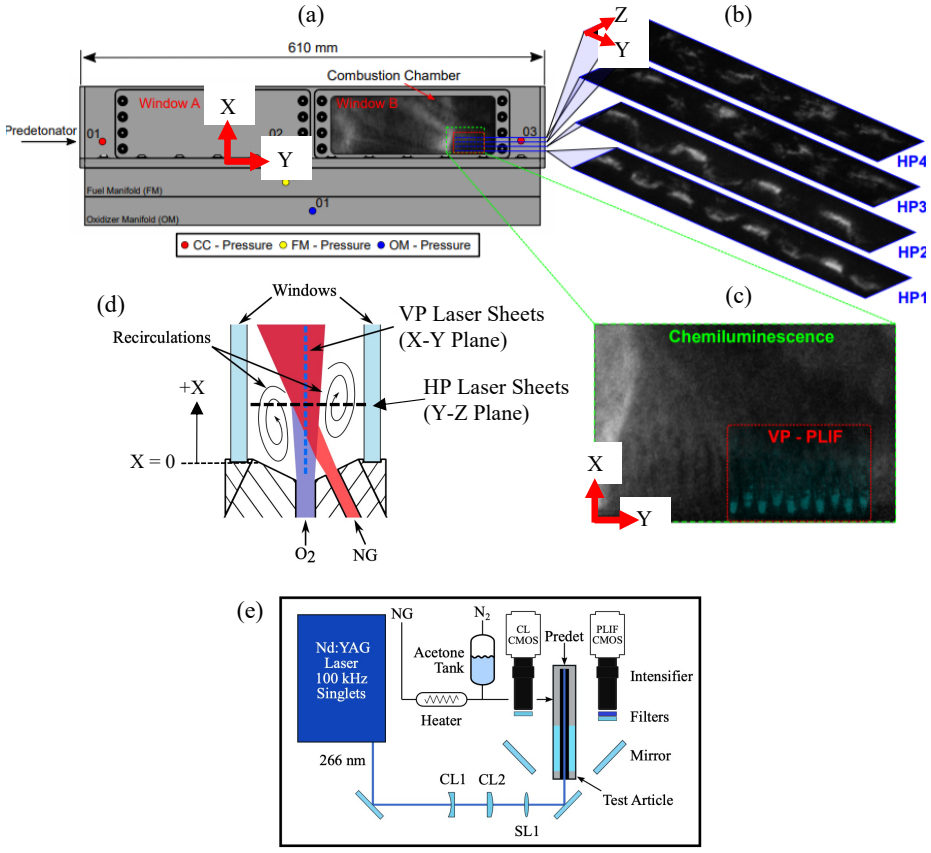

Figure 20. Linear RDE diagnostic layout. (a) Test rig schematic showing imaging fields of view. (b) Y-Z HP acetone PLIF measurement planes. (c) X-Y VP acetone PLIF measurement planes with overlapping OH* chemiluminescence. (d) Schematic showing placement of acetone PLIF planes in the test rig. (e) Optical layout schematic showing laser, optics, and imaging systems.

100 kHz Fuel PLIF in the linear RDC (X-Y Plane):

A time series of raw (no image post processing beyond the dot target calibration) 100 kHz acetone-PLIF images extracted during a time interval representative of limit-cycle engine operation is shown in Figure 21. The image series begins with the fuel refill process immediately after a detonation wave has exited the right-side of the FOV. The first several images display a fuel refill process. Namely, a majority of the acetone-PLIF signal is depleted behind the detonation wave within a high-pressure gas region which enforces a temporary cessation of fuel injection. After fuel injection resumes, fuel jet fronts are observed to form an upward slope in the direction opposite the wave propagation direction. However, several distinctive reactant injection and mixing processes unique to the injection scheme and operating condition presented in the Figure 21 time series are apparent. One of the jets in the center of the frame shows no evidence of recovery until 61.00 ms, while jets to the left and right have begun the refill process 20 μs earlier.

Fundamentally, the acetone fluorescence signal can disappear for two primary reasons:

- Acetone pyrolysis occurs above temperatures of approximately 700 K. This can be achieved through increased mixing of the fuel stream with hot combustion products, thus raising the local temperature to above 700 K.
- Deflagration of the fuel locally, consuming the acetone. In this case, either the hydrocarbon acetone is consumed too, or the natural gas fuel is consumed raising the local temperature above the acetone pyrolysis temperature.

One striking feature of these images is the number of acetone fluorescence structures that are preserved behind the detonation front and near the injector face, indicating pockets of unburned fuel. The frames at 61.11 ms and 61.12 ms reveal that before these pockets of fuel are fully consumed, they detach from the injector face, revealing the cessation of fuel injection. These small regions with PLIF signal containing, notionally, poorly mixed fuel quickly disappear likely from rapid mixing with the surrounding hot combustion products and/or burning.

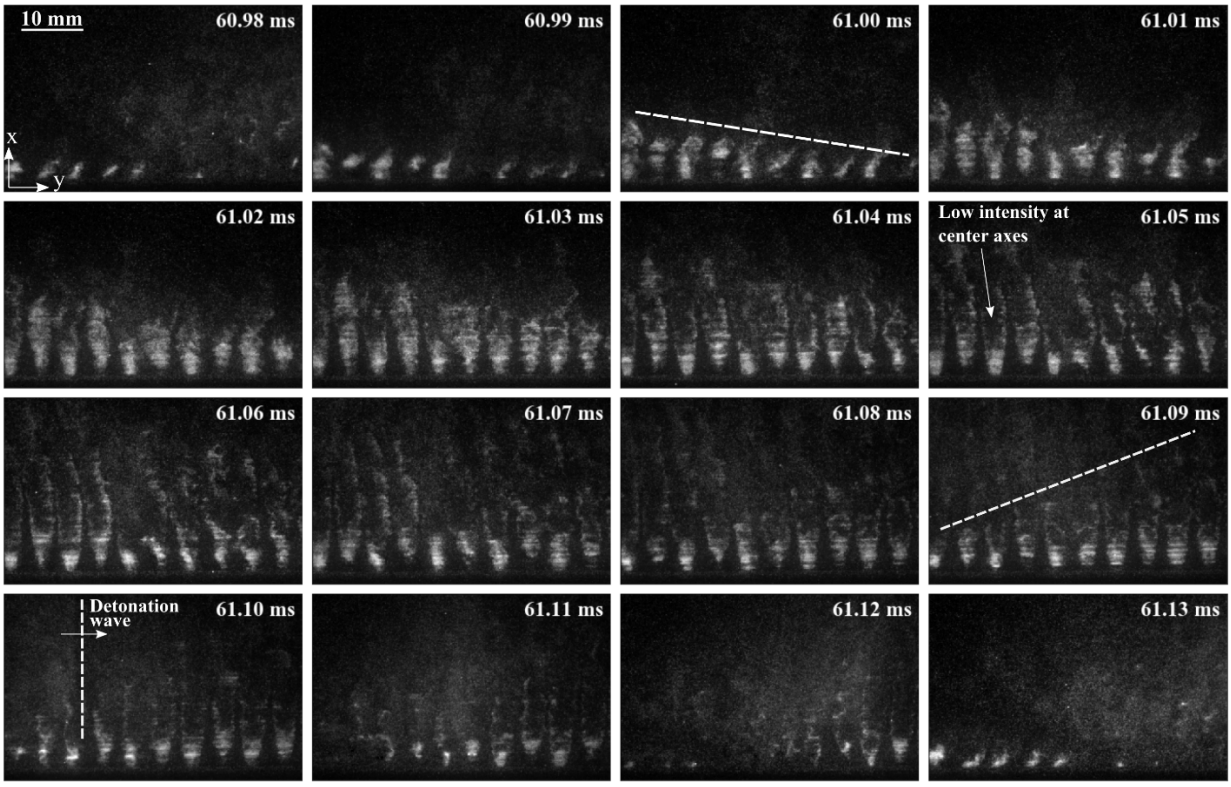

Figure 21. Raw 100 kHz acetone-PLIF images from a single detonation cycle of Case A (detonation propagation is left to right).

100 kHz Simultaneous Fuel PLIF (X-Y Plane) and OH* Chemiluminescence Imaging in the linear RDC:

Figure 22 shows simultaneous Fuel-PLIF and OH* chemiluminescence imaging for one passage of the detonation wave. The chemiluminescence images reveal a forward leaning detonation wave with a trailing heat release zone. The detonation wave front combustion intensity is lower near the injector face, coincident with the alternating pattern of high and low fuel concentrations, suggesting that poor mixing near the injector face results in a locally weakened detonation wave. This poorly-mixed injector nearfield is further corroborated by the observed fuel jet structures that remain behind the detonation wave, indicating that pockets of high fuel concentration near the injector face are not fully consumed at the detonation front. Another notable characteristic in Figure 22 is a band of low heat release behind the detonation wave (outlined at 61.65 ms, between the white dashed lines). At the detonation front, this low heat release band is coincident with the top of the fuel refill height (note the fuel jet front projections from the PLIF, white and

green circles in Figure 22) and the start of the oblique shock. Additional analysis supports that this suggests that a fuel-rich, noncombustible layer exists at the top of the refill zone. First, this low heat release layer becomes less pronounced for the leaner equivalence ratio cases (not shown). This is consistent with longer measured fuel injector recovery times for the leaner equivalence ratio cases, arising from lower fuel injection pressures than those seen in other cases considered. Second, the fuel jet behavior about the z= 0 plane

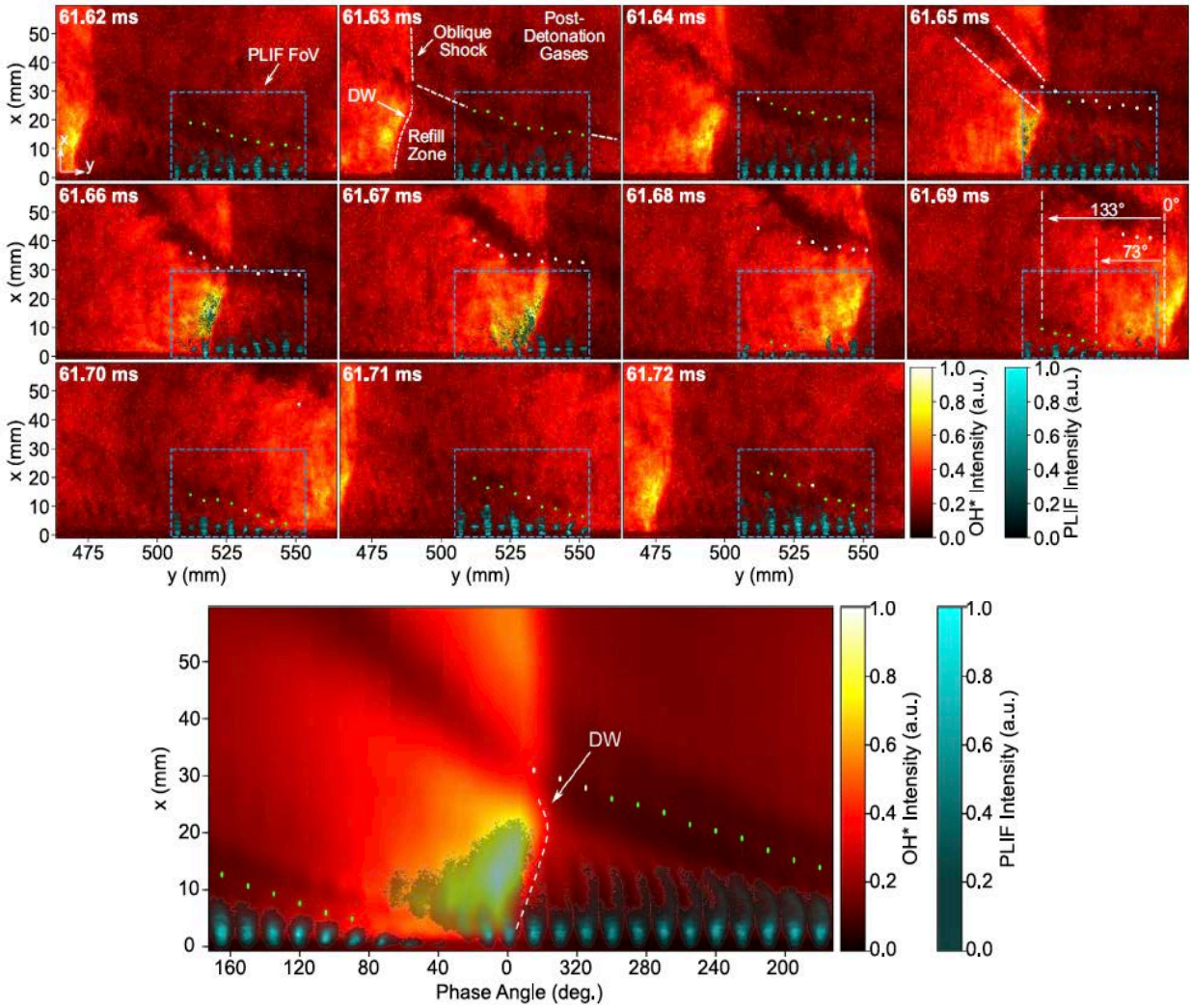

Figure 22. Simultaneous fuel PLIF and OH* chemiluminescence imaging. Top: short time sequence showing the detonation wave entering the PLIF field of view. Bottom: cycle phase averaged fuel PLIF and OH*.

indicates that as soon as the fuel jets recover, the fuel penetration depth across the channel (z-direction) is larger than later in the cycle, indicating that the oxidizer flow exhibits a longer recovery time than the fuel. In essence, the fuel injector is recovering faster.

The phase-averaged OH∗ chemiluminescence and acetone-PLIF for Case D is also shown in Figure 22. Similar characteristics are observed in the phase-averaged field as were also observed in the instantaneous fields in Figure 22. The detonation wave displays a forward lean, an oblique shock, and unburned fuel remaining behind the detonation wave that is more pronounced near the injector. Fuel jet front location measurements reveal an approximately linear fuel refill height and a projected average fuel refill height at the detonation wave of 31 mm. The phase-averaged fuel refill height projections confirm that the fresh fuel supply at the top of the fuel refill intersects the detonation wave at the upper x -boundary of the non-reacting layer that continues behind the detonation wave. This result further supports the hypothesis that this layer of low heat release is a fuel-rich and non-reacting zone.

Fuel Injection Recovery Time Scaling

A region near the injection surface was monitored to quantify the fuel injector recovery time. Figure 23 (a) provides average fuel injector recovery times, rec , across a range of operating conditions. The fraction of fuel recovery time relative to a detonation wave period, cycle = 1 / f_{LC} , is shown on the second Y-axis. Fuel injector recovery times varied between 11–24 μs across the range of operating conditions considered, monotonically decreasing with increasing equivalence ratio. The trends in Figure 23 (a) mask a complicated dependence of the fuel recovery time on other parameters, since as the equivalence ratio changes other measured parameters are also changing (such as detonation wave frequency, detonation strength, and injector manifold pressures). To account for the effect of these additional parameters, a parameter ( ) representing the ratio of P to the average fuel injector pressure drop is defined (see Eq. (1)). This approach accounts for the mean injector stiffness and the impulse strength of the detonation wave. As shown in Figure 23 (b), exhibits a linear relationship with the fuel injector recovery time. While this confirms that the detonation wave strength and injector stiffness appear to be leading order parameters that influence the fuel injector recovery time (an expected result), the actual functional relationship of the fuel recovery time with these parameters has not been previously well detailed. Moreover, this represent one of only two experimental quantifications of fuel injector recovery times in an RDC device, with the first instance performing measurements at only a 10-Hz-rate.

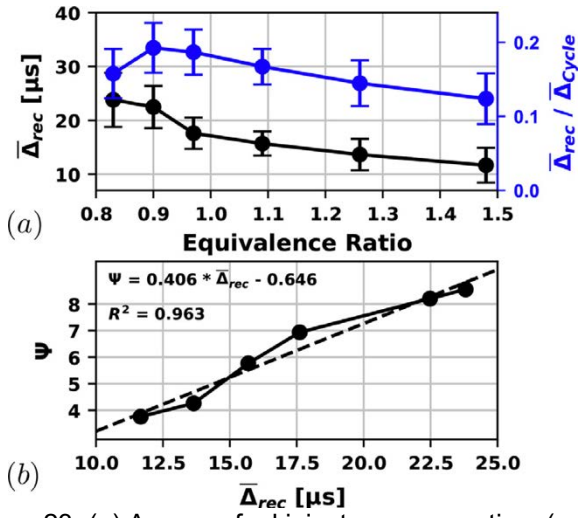

Figure 23. (a) Average fuel injector recovery time (_*rec*) and (b) the ratio of average peak detonation wave cycle pres- sure rise to average injector pressure drop (_) as a func- tion of fuel injector recovery time.

SUMMARY AND CONCLUSIONS

Advanced laser-based imaging measurements were applied to two optically-accessible RDC experiments to spatially and temporally resolve various injector, mixing, combustion, and detonation flow processes. All of these measurements are performed at ultra-high repetition rates (100 kHz to 2 MHz) and uniquely enabled by the high-power, high-speed burst mode lasers, and in some cases in combination with custom-built high-speed optical parametric oscillators.

This paper provided a high-level and broad survey of some of the advanced diagnostics applied in these RDCs. We have explored and demonstrated a wide range of diagnostics to investigate various aspects of the RDC, such as:

- **(Annular RDC) Liquid injection behavior:** Demonstrated liquid fuel 355-nm PLIF to visualize the time-dependent liquid fuel injection process up to a 1 MHz imaging rate. For this, the annular RDC is used as a detonation driver to impose periodic detonation waves to interact with the fuel spray.
- **(Annular RDC) Detonation structure and combustion behavior:** Demonstrated 2 MHz OH-PLIF imaging, extending the technique to multiple simultaneous laser planes for three-dimensional information.
- **(Annular RDC) Air injector behavior:** we have been exploring various laser-based air-stream visualization tracer methods over a range of repetition rates (100 kHz – 1 MHz). While some of the demonstrated approaches are more challenging and likely warrant further study for improvement (e.g., NO_2-PLIF), other more conventional approaches such as gaseous acetone tracing for acetone-PLIF seem to work well enough for the intended purpose of characterizing the injector behavior.

- **(Linear RDC)** In the linear RDC, we explored and demonstrated up to 200 kHz fuel PLIF for mixing by tracing small amounts of acetone in the fuel supply. This technique was then extended to two laser sheets orthogonal to the original investigated plane to derive three-dimensional fuel mixing details.

ACKNOWLEDGMENTS

This work was funded by NASA STTR contracts 80NSSC19C0551 and 80NSSC21C0031 (T.M. Doug Perkins). Portions of the imaging equipment used for the annular RDC work was provided, in part, under AFOSR Award No. FA9550-16-1-0315, DTRA Award No. HDTRA1-17-1-0031, and DOE Award No. DE-FE0032075. Portions of the imaging equipment used for the linear RDC work was purchased with DURIP grant FA9550-16-1-0534 and Defense Threat Reduction Agency Award HDTRA1-17-1-0031.

REFERENCES

1. Fry, R. S. and Peters, S. T., ***Burning Rates of Standard Solid Propellants for Gun Applications***, CPTR 99-69, CPIA/JHU, Columbia, MD (Sep 1999).

---

[i] Meyer, Terrence R., Michael Brear, Seong Ho Jin, and James R. Gord. "Formation and diagnostics of sprays in combustion." *Handbook of Combustion: Online* (2010): 291-322.

[ii] Zhang, Yinchao, Ting Li, He Chen, Siying Chen, Pan Guo, and Yi Li. "Excitation wavelength analysis of a laser-induced fluorescence technique for quantification of extra virgin olive oil adulteration." *Applied optics* 58, no. 16 (2019): 4484-4491.